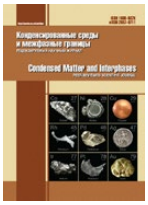

ISSN 1606-867X (Print)
ISSN 2687-0711 (Online)
Condensed Matter and Interphases
Kondensirovannye Sredy i Mezhfaznye Granitsy
https://journals.vsu.ru/kcmf/

Original articles

Research article
https://doi.org/10.17308/kcmf.2025.27/13181

Photoluminescent properties of porous silicon nanoparticles: synthesis, characterization, and cellular imaging

D. A. Nazarovskaia[1], S. Yu. Turishchev[2], S. S. Titova[2], A. A. Shatov[1], P. A. Tyurin-Kuzmin[1,3], L. A. Osminkina[1,3]✉

[1]Lomonosov Moscow State University,
1 Leninskie Gory, Moscow 119991, Russian Federation

[2]Voronezh State University,
1 Universitetskaya pl, Voronezh, 394018, Russian Federation

[3]Institute for Biological Instrumentation of the Russian Academy of Sciences,
7 Institutskaya st., Pushchino 142290, Russian Federation

Abstract

Objective: This study investigates the stability of photoluminescent (PL) properties of microporous silicon nanoparticles (μpSi-NPs) synthesized by electrochemical etching of monocrystalline silicon followed by lyophilization.

Experimental: Structural analysis revealed a highly porous architecture with < 2-nm pores and silicon nanocrystals (nc-Si) with an average size of 3–5 nm. Fourier-transform infrared spectroscopy confirmed the presence of Si-O-Si bonds, indicating surface oxidation of nc-Si. PL studies demonstrated a broad emission band peaking at 685 nm, attributed to exciton recombination in nc-Si. After 5 months of storage, the PL peak shifted to 655 nm, reflecting oxidation-induced size reduction of nc-Si. Raman spectra showed a 1.5 cm^{-1} shift of the Si phonon peak along with spectral broadening, evidencing phonon confinement and partial amorphization. XANES analysis further confirmed increased suboxide content and structural disorder.

Conclusions: Biological experiments demonstrated the biocompatibility of μpSi-NPs and retention of their PL activity, highlighting their potential for biomedical applications such as bioimaging and biosensing.

Keywords: Porous silicon, Lyophilization, Photoluminescence, XANES, Raman scattering, Bioimaging

Funding: This work was supported by Russian Science Foundation grant No. 24-15-00137 (https://rscf.ru/project/24-15-00137/) for nanoparticle synthesis and structural characterization Lomonosov Moscow State University grant No. 23-SCH06-19 for cellular imaging studies, BASIS Foundation grant No. 23-2-2-18-1 for optical properties investigation.

Acknowledgments: The research utilized equipment from the Lomonosov Moscow State University Shared Facilities Center «Technologies for Obtaining New Nanostructured Materials and Their Comprehensive Study».

For citation: Nazarovskaia D. A., Turishchev S. Yu., Titova S. S., Shatov A. A., Tyurin-Kuzmin P. A., Osminkina L. A. Photoluminescent properties of porous silicon nanoparticles: synthesis, characterization, and cellular imaging. *Condensed Matter and Interphases*. 2025;27(3): 422–432. https://doi.org/10.17308/kcmf.2025.27/13181

Для цитирования: Назаровская Д. А., Турищев С. Ю., Титова С. С., Шатов А. А., Тюрин-Кузьмин П. А., Осминкина Л. А. Фотолюминесцентные свойства наночастиц пористого кремния: синтез, характеризация и визуализация в клетках. *Конденсированные среды и межфазные границы*. 2025;27(3): 422–432. https://doi.org/10.17308/kcmf.2025.27/13181

✉ Liubov A. Osminkina, e-mail: osminkina@physics.msu.ru

1. Introduction

The photoluminescence (PL) of porous silicon (pSi) was first discovered in the early 1990s, generating significant scientific interest due to its potential applications in optoelectronics and biomedicine [1]. However, the practical applications of pSi have been limited by the temporal instability of its PL properties, primarily caused by surface oxidation under ambient conditions. This oxidation leads to a gradual reduction in PL intensity and spectral shifts. Various surface passivation techniques have been developed to address this issue, including chemical modification, thermal oxidation, and polymer coating, all aimed at protecting the silicon surface and preserving its optical properties. The choice of an appropriate stabilization method depends on specific operational requirements and desired material characteristics.

Porous silicon nanoparticles (pSi-NPs) exhibit considerable potential for diverse biological applications, particularly in biosensing [7, 8], targeted drug delivery [9], and novel therapeutic approaches involving controlled interactions with cells and tissues [10, 11]. Their biomedical utility derives from several advantageous properties: excellent biocompatibility, low cytotoxicity, tunable biodegradation rates, and a highly porous structure with large surface area that facilitates efficient drug loading and surface functionalization [12].

The PL phenomenon in pSi-NPs originates from quantum confinement effects in silicon nanocrystals typically ranging from 2 to 7 nm in size. This spatial restriction of charge carriers leads to bandgap widening and a shift of the emission spectrum into the visible range, predominantly the red-orange region. Surface characteristics, including defects and chemical termination (hydride or oxide groups), significantly influence both the intensity and the spectral profile of PL emission [13–15].

These unique optical properties enable various biomedical applications, particularly in diagnostic imaging where pSi-NPs serve as effective contrast agents. Their strong luminescence and broad excitation spectrum allow tracking of cells and tissues using conventional fluorescence microscopy techniques, both *in vitro* and *in vivo* [16–18].

The pore size critically determines the physicochemical and functional properties of pSi-NPs. Microporous structures (pores < 2 nm) exhibit rapid biodegradation under physiological conditions, which limits their applicability for long-term delivery but makes them useful for short-term therapeutic applications. Mesoporous materials (pores 2–50 nm) provide an optimal balance between degradation rate and loading capacity for therapeutic molecules such as drugs, proteins, and DNA. Macroporous variants (pores > 50 nm) are mainly used in photonics, filtration, and other engineering applications due to their large pore size and limited capacity to effectively retain bioactive molecules [15].

During fabrication, nanoscale pores can generate substantial capillary forces during solvent evaporation, potentially reaching pressures exceeding 100 MPa in 2 nm pores according to the Laplace equation ($\Delta P = \frac{2\alpha}{r}$), where ΔP is the pressure difference between the liquid and vapor phases, α is the surface tension coefficient of the liquid, and r is the pore radius. These forces often produce structurally heterogeneous and mechanically fragile materials. Lyophilization has emerged as an effective processing technique that maintains structural integrity while enabling production of highly porous (> 90 %) materials with enhanced PL characteristics. XANES studies have confirmed that lyophilization effectively limits surface oxidation to superficial layers (2–3 nm), preserving the optical properties over extended storage periods [20, 21].

The current study focuses on a comprehensive characterization of microporous silicon nanoparticles produced by electrochemical etching and lyophilization, with particular emphasis on analyzing surface composition and evaluating optical properties. Special attention is given to assessing the stability of these properties during air exposure, as this critically determines their suitability for biological imaging applications. The investigation combines

advanced spectroscopic techniques with morphological analysis to establish structure–property relationships essential for optimizing biomedical performance.

2. Experimental

2.1. Synthesis of microporous silicon films

Microporous silicon films (μPSi) were synthesized by electrochemical etching of monocrystalline silicon wafers (c-Si) with (100) orientation and resistivity of 10 Ω·cm. To ensure uniform and reproducible etching, a thin aluminum layer was deposited on the backside of the wafers to serve as an ohmic contact. The silicon etching was performed in a 1:1 mixture of concentrated HF (48 %) and ethanol at 50 mA/cm^2 for 30 minutes. The resulting films were delaminated in a 1:20 HF:ethanol solution at 4 mA/cm^2 for 250 seconds [22].

2.2. Lyophilic drying

The μpSi films were rinsed with deionized water (three washing cycles) to remove residual acid and then lyophilized for 12 h using a benchtop freeze-dryer (Advantage 2.0 ES-53). The dried μpSi powder were stored in sealed glass containers at room temperature in the dark.

2.3. Characterization of optical properties

The surface chemical composition of μpSi powder was studied using an IR-8000 Fourier-transform infrared spectrometer equipped with a diamond ATR accessory in the range of 400–4000 cm^{-1}. Raman scattering and PL spectra of the samples were measured with a Confotec™ MR350 confocal Raman microscope. Raman spectra were recorded using 785 nm laser excitation at a low power of 1 mW to avoid sample overheating, with an acquisition time of 60 s per spectrum. PL spectra were acquired under 488 nm laser excitation with an exposure time of 10 s.

2.4. Structural analysis by XANES spectroscopy

X-ray absorption near-edge structure (XANES) spectroscopy was employed to study the local atomic environment and electronic structure of nanoparticles. Si $L_{2,3}$-edge and O K-edge XANES spectra were collected using high-intensity radiation from a "megascience"-class synchrotron source (KISI-Kurchatov synchrotron, NanoPES beamline, NRC "Kurchatov Institute", Moscow, Russia) [29], enabling tunable X-ray energies without intensity loss. XANES provides information about the local partial density of unoccupied electronic states in the conduction band [23, 24], exhibiting exceptional sensitivity to atomic coordination environments [25–28]. The analysis depth was ~5 nm for Si $L_{2,3}$ spectra [30] and ~10 nm for O K spectra [31], with instrumental broadening of 0.1 eV. Experiments were conducted at ~10^{-10} Torr vacuum, detecting total electron yield (TEY) via sample drain current. The synchrotron beam incidence angle was 90° to the surface plane, with samples mounted on Omicron flag-type holders for charge dissipation. Reference spectra were acquired from:crystalline silicon (c-Si),amorphous silicon on Si (a-Si) with native SiO_2 (<2 nm), thermal SiO_2 film on Si (20 nm).

2.5. Nanoparticle preparation and morphology studies

For luminescent labeling applications, lyophilized μpSi films were fragmented into nanoparticles (μpSi-NPs) using a FRITSCH Pulverisette 7 premium line planetary mill (30 min in ethanol). The resulting suspensions were sedimented for 24 hours to remove large particles, with the supernatant used for experiments.

Morphology and size distribution of μpSi-NPs were characterized by transmission electron microscopy (TEM, LEO 912 AB, 100 kV accelerating voltage). For TEM imaging, ethanol suspensions of μPSi-NPs were drop-cast onto 3 mm copper grids with carbon support films and vacuum-dried for 10 minutes.

2.6. Confocal luminescence microscopy

Mesenchymal stem cells (MSCs) were isolated from human abdominal subcutaneous adipose tissue obtained during bariatric surgeries performed at the Medical Research and Education Center of Lomonosov Moscow State University. All donors were female with a mean age of 39±7 years and a body mass index of 22±1. Written informed consent was obtained from

each participant, and the study protocol was approved by the Local Ethics Committee of the Medical Research and Education Center (IRB00010587, Moscow, Russia; Protocol No. 4, June 4, 2018). Adipose tissue samples (0.5–5 mL) were homogenized and digested in a solution containing Collagenase I (200 U/mL, Worthington Biochemical, USA) and Dispase (40 U/mL, Sigma-Aldrich, USA) with continuous agitation for 30–40 minutes at 37 °C. The digested tissue was centrifuged at 200×g for 10 minutes, after which the supernatant was discarded. The pellet containing MSCs was subjected to hypotonic lysis to remove erythrocytes, filtered through a 100-µm cell strainer (BD Falcon, USA), and centrifuged again at 200×g for 10 minutes. The final pellet was resuspended in culture medium for further expansion.

MSCs were cultured in low-glucose DMEM (1 g/L, PanEco, Russia) supplemented with 10 % fetal bovine serum (HyClone, Cytiva, USA) and 1 % antibiotic-antimycotic solution (HyClone, Cytiva, USA). Cells were maintained at 37 °C in a 5 % CO_2 incubator (Binder, Tuttlingen, Germany) and passaged at 80–90 % confluency using Versene (PanEco, Russia) and trypsin (PanEco, Russia). MSCs at passages 5–6 were used for experiments. To confirm their multipotency, the cells were stained for surface markers CD73, CD90, CD105, and CD34 and induced to differentiate into osteogenic, adipogenic, and chondrogenic lineages as previously described [34].

For microscopy, cells were seeded in confocal dishes and allowed to adhere overnight. µpSi-NPs were then added and incubated with the MSCs for 10 hours prior to imaging. The intracellular localization of the nanoparticles was visualized using a Zeiss LSM780 confocal microscope equipped with a Plan-Apochromat 63×/1.40 Oil DIC objective. Luminescence was excited using a 405 nm diode laser, and the intrinsic luminescence of the nanoparticles was detected in the 409–700 nm range with a pinhole setting of 1 au.

3. Results and discussion

Fig. 1 presents a TEM micrograph showing the morphology of the synthesized µPSi-NPs

The image confirms the presence of a well-developed porous structure in the material. The size of individual nanoparticles is estimated to be in the range of 100–200 nm. The micrograph also reveals non-uniform pore structure, which may be attributed to the synthesis conditions and lyophilic drying process.

Fig. 2 displays the FTIR transmission spectrum of µpSi, showing characteristic absorption bands associated with Si-O-Si groups. The band at approximately 460 cm^{-1} corresponds to rocking vibrations of Si-O-Si bonds, while the band near 840 cm^{-1} indicates symmetric stretching vibrations. Asymmetric stretching vibrations of Si-O-Si are observed at 1050 cm^{-1}, confirming the presence of an oxide surface formed during lyophilic drying and subsequent air storage of the samples.

Fig. 3 shows the Si $L_{2,3}$-edge XANES spectra of reference samples (crystalline silicon c-Si, amorphous silicon a-Si, and thermal $L_{2,3}$ film) and the studied µPSi powder.

The crystalline silicon (c-Si) spectrum exhibits distinct fine structure (region A) associated with the 0.6 eV spin-orbit splitting of silicon's $L_{2,3}$ core level. This characteristic feature reflects the high degree of atomic ordering in the c-Si lattice.

Region A of the amorphous silicon reference exhibits simpler fine structure due to the blurring of electron density states. In the energy

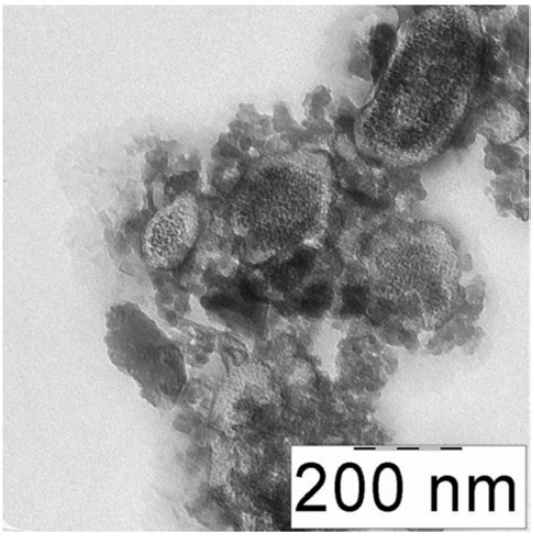

Fig. 1. TEM micrograph of µPSi-NPs

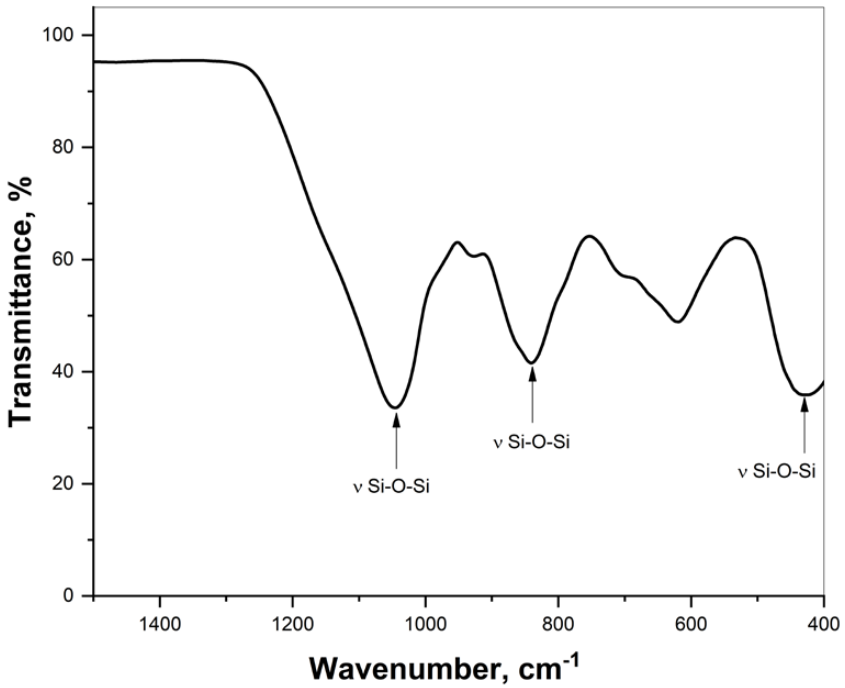

Fig. 2. FTIR transmission spectrum of μpSi powder. The absorption bands correspond to the stretching vibrations of Si-O-Si bonds

range of synchrotron radiation up to 104 eV, the absorption edge is absent for the reference thermal SiO_2 film. However, for the studied μPSi powder, the absorption edge is clearly detected ($h\nu$ < 104 eV) though lacking distinct fine structure features A characteristic of crystalline c-Si, while showing higher intensity than the a-Si reference (Fig. 3b). This indicates certain disordering in the silicon atomic network, whose signal nevertheless remains present in the recorded spectra.Comparative analysis of fine structures in reference spectra of c-Si and a-Si (with native oxide) along with thermal SiO_2 film reveals that for synchrotron radiation energies above 104 eV (characteristic features B and C), the powder spectrum generally corresponds to silicon atoms bonded to oxygen atoms. Notably, the μPSi powder spectrum (Fig. 3a) shows relative intensity enhancement in the 104–105 eV range compared to references. Such spectral intensity elevation typically indicates contributions from silicon suboxides in the surface layer of μPSi [25, 28]. Deviation from SiO_2 stoichiometry is further evidenced by altered intensity ratios of features B and C in μPSi compared to references. Additionally, the broadened feature C (Fig. 3b) suggests possible silicon suboxide contributions. An extra spectral feature around 108 eV (near feature C) results from partial surface charging during leakage current (sample current) measurements. Previous studies [36, 37] have reported various «intensity inversion» effects in Si $L_{2,3}$ XANES fine structures, attributed to interaction phenomena between synchrotron radiation and silicon-based structures.

The O K-edge XANES spectra (Fig. 3b) for thermal SiO_2 film and μPSi powder demonstrate that while the positions and relative intensity distributions of main features A, B, and C indicate predominant SiO_2 coating on powder particles, the enhanced intensity of feature A reveals deviations from stoichiometric SiO_2 [38, 39], consistent with Si $L_{2,3}$ edge spectroscopy data.

Thus, the Si $L_{2,3}$ and O K-edge XANES spectra (Fig. 3) demonstrate that μPSi is characterized by: disordering of the silicon atomic lattice, the presence of suboxides, deviation from stoichiometric SiO_2 composition. These features indicate a complex and heterogeneous surface structure of the samples.

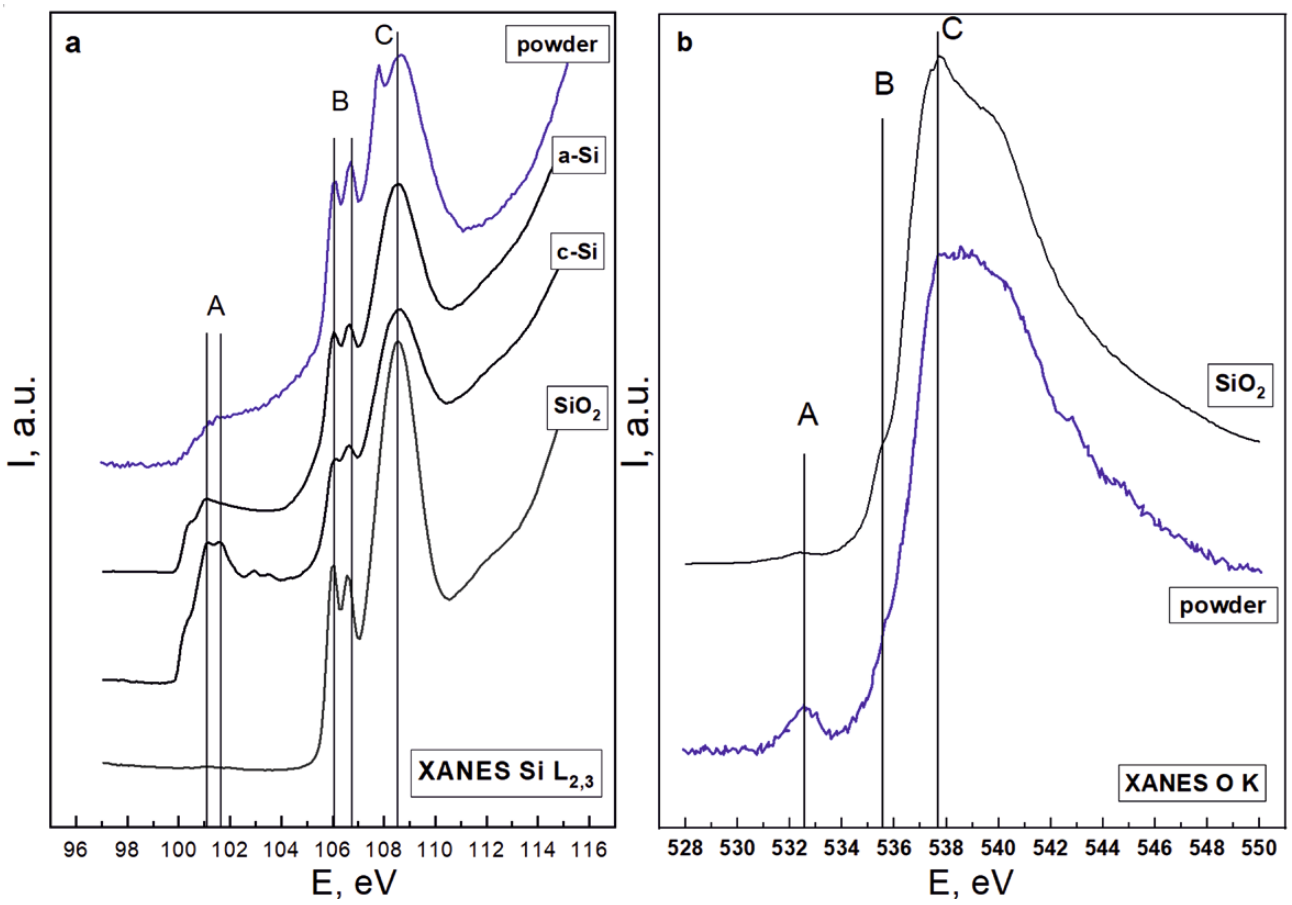

Fig. 3. (a) Si $L_{2,3}$ -edge XANES spectra of μPSi powder and reference samples: crystalline silicon (c-Si), amorphous silicon (a-Si), and thermal SiO_2 film. Regions A, B, and C correspond to features associated with silicon atoms and their bonding with oxygen. (b) O K-edge XANES spectra of μPSi powder and thermal SiO_2 film. The relative intensity increase of feature A in the powder indicates deviations from stoichiometric SiO_2 composition

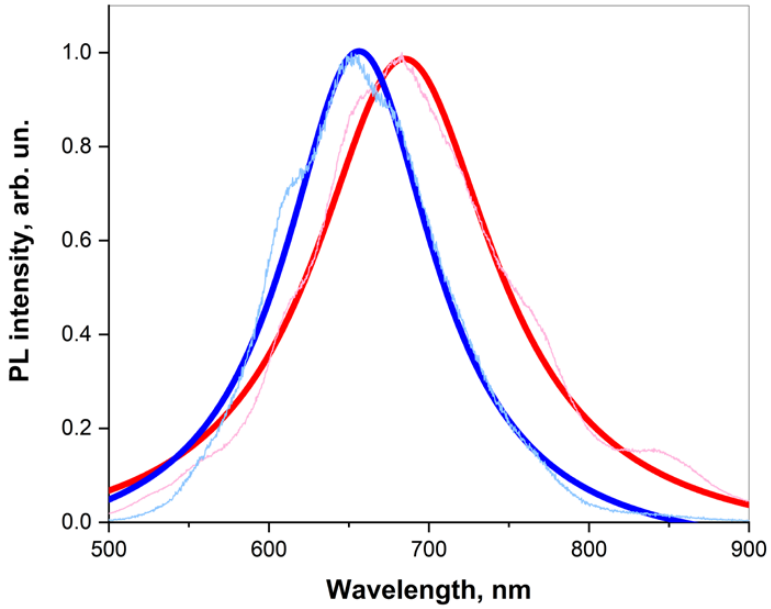

Fig. 4. PL spectra of μPSi powder: freshly prepared samples (red) and after 5 months of air storage (blue). Thick lines represent Lorentzian fitting of experimental spectra (thin lines)

Fig. 4 shows the PL spectrum of μPSi powder for freshly prepared samples (red curve) and after 5 months of air storage (blue curve).

The spectrum of freshly prepared samples exhibits a broad band with a maximum at 685 nm, which is attributed to radiative exciton annihilation in silicon nanocrystals (nc-Si). The spectral broadening is explained by the size distribution of nanocrystals, which is typical for such materials.

The position of the PL maximum correlates with the average nanocrystal size d according to the empirical formula [3]:

$$E(d) = E_0 + \frac{3.73}{d^{1.39}}, \quad (1)$$

where E_0 is the band gap of c-Si (1.12 eV). The average nanocrystal diameter in freshly prepared samples, calculated from PL spectra using formula (1), was determined to be 3.8 nm.

After 5 months of storage, the spectrum shows a blue shift (maximum at 655 nm), indicating a reduction in the average nanocrystal size to 3.3 nm. This effect can be explained by gradual oxidation of silicon nanocrystals in air, leading to an increased oxide phase fraction and reduction of their effective size.

Fig. 5 presents Raman spectra for freshly prepared μPSi powder (a) and after 5 months of air storage (b). The intense peak in both spectra corresponds to phonon scattering from the silicon lattice. Due to quantum confinement of phonons in small-sized nc-Si, the observed peak is shifted to lower frequencies relative to the value for c-Si (520.5 cm^{-1}) by $\Delta\omega$ = 1.5 cm^{-1}. This confirms the presence of silicon nanocrystals in the sample structure.

For precise peak position determination, the spectra were fitted with Lorentzian functions, enabling calculation of the average nanocrystal size using the empirical formula [40]:

$$d = 0.543\left(\frac{52.3}{\Delta\omega}\right)^{0.63}. \quad (2)$$

The calculated average diameter of nanocrystals in freshly prepared samples was 5.3 nm. After air storage, the Raman peak position remains virtually unchanged, indicating preservation of the overall nanocrystal size. However, spectral broadening with formation of

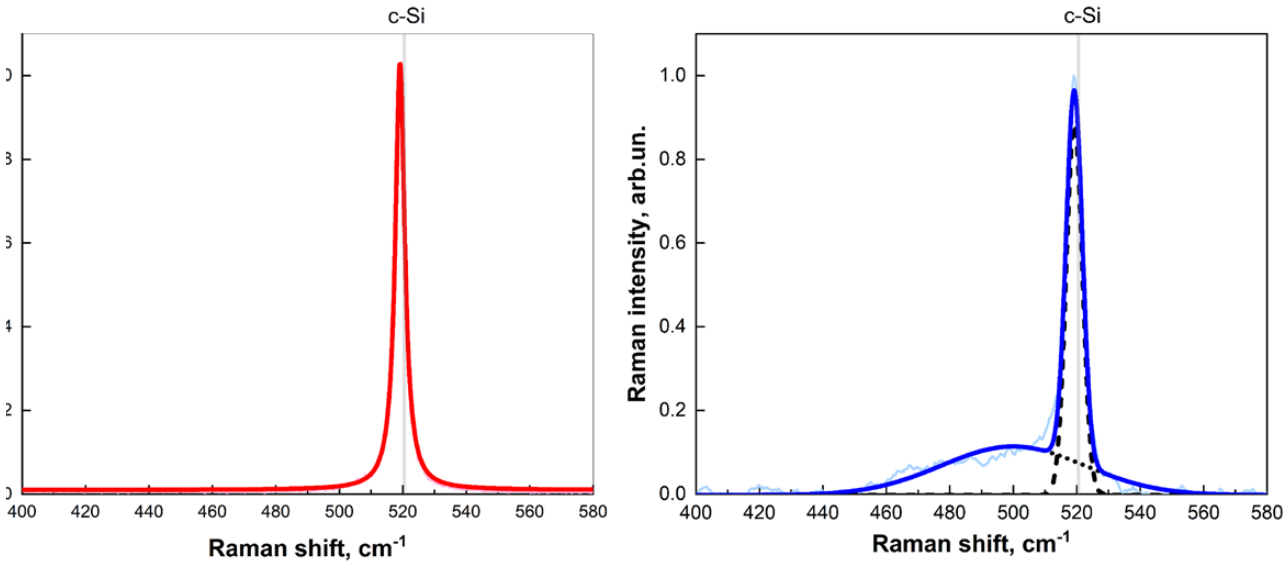

a b

Fig. 5. Raman spectra of μPSi powder: (a) freshly prepared and (b) after 5 months of air storage. In (a), the thick line represents Lorentzian fitting of the experimental spectrum (thin line). In (b), the thick line shows the fitting and sticks represent the deconvolution of the experimental spectrum (thin line)

a low-frequency shoulder is observed, associated with partial amorphization of nanocrystals due to surface oxidation [41].

Spectral deconvolution allowed estimation of phase composition: the crystalline and amorphous fractions of the powder after storage were 46.3% and 53.7%, respectively. These changes confirm that surface oxidation leads to structural heterogeneity accompanied by partial loss of crystalline ordering.

It should be noted that the discrepancy between nc-Si sizes calculated from PL and Raman data arises from the different sensitivities of these techniques to surface processes, oxidation state, and phase composition of nanocrystals. PL reflects an average «effective» size including oxidation effects, while Raman characterizes the dimensions of the ordered part of the material crystal lattice.

The photoluminescent properties of μPSi-NPs enable their use as fluorescent labels for cell visualization. Figure 6 shows microscopy images of MSCs (mesenchymal stem cells) after 10 hours of incubation with μPSi-NPs.

Fig. 6b clearly demonstrates the efficient luminescence of μPSi-NPs localized in the cell cytoplasm, indicating that the particles retain their PL properties upon incubation with cells.

4. Conclusions

In this work, the morphological, structural, and optical properties of μPSi-NPs synthesized by electrochemical etching followed by lyophilization were investigated. Transmission electron microscopy, infrared spectroscopy, and Raman spectroscopy revealed that μPSi powders possess a well-developed porous architecture with silicon nanocrystals of about 4–5 nm in size. The surface of the samples was found to contain oxide groups, as confirmed by IR and XANES spectroscopy.

PL analysis showed that the nanocrystals retain their luminescent properties after 5 months of storage in air. Nevertheless, a blue shift of the PL peak was observed, associated with a reduction in the effective nanocrystal size, most likely due to surface oxidation. Raman spectra further indicated partial surface amorphization of the nanocrystals during storage, manifested by spectral broadening and the appearance of a low-frequency shoulder, which is consistent with oxidation processes. The PL properties of μPSi-NPs, which remain stable during interaction with mesenchymal stem cells, confirm their promise for bioimaging and biosensing applications.

Importantly, the findings demonstrate that lyophilization is an effective method for preserving the structural and optical characteristics of μPSi-NPs during storage, thereby supporting their suitability for future biomedical and optical applications.

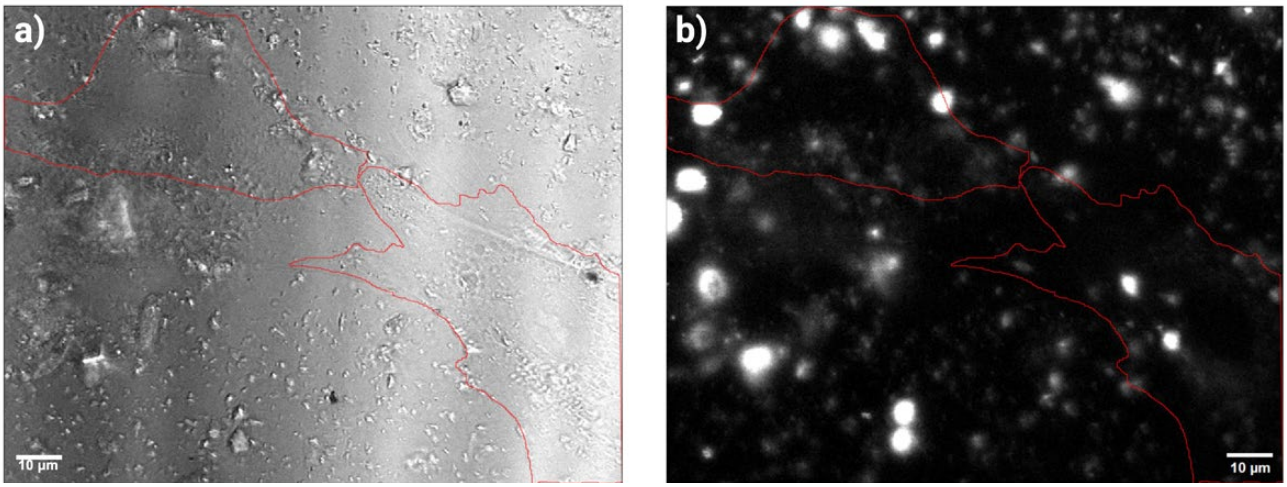

Fig. 6. Microscopy images of live MSCs after 10 h of incubation with μPSi-NPs: (a) bright-field image; (b) photoluminescence image. Red lines outline the cell borders. Scale bar: 10 μm

Contribution of authors

The authors contributed equally to this article.

Conflict of interests

The authors declare that they have no known competing financial interests or personal relationships that could have influenced the work reported in this paper.

References

1. Cullis A. G., Canham L. T. Visible light emission due to quantum size effects in highly porous crystalline silicon. *Nature*. 1991;353(6342): 335–338. https://doi.org/10.1038/353335a0

2. Lauerhaas J. M., Sailor M. J. Chemical modification of the photoluminescence quenching of porous silicon. *Science*. 1993;261(5128): 1567–1568. https://doi.org/10.1126/science.261.5128.1567

3. Gongalsky M. B., Kargina J. V., Cruz J. F., ... Sailor M. J. Formation of Si/SiO_2 luminescent quantum dots from mesoporous silicon by sodium tetraborate/citric acid oxidation treatment. *Frontiers in Chemistry*. 2019;7: 165. https://doi.org/10.3389/fchem.2019.00165

4. Salonen J., Mäkilä E. Thermally carbonized porous silicon and its recent applications. *Advanced Materials*. 2018;30(24): 1703819. https://doi.org/10.1002/adma.201703819

5. Erogbogbo F., Yong K. T., Roy I., Xu G., Prasad P. N., Swihart M. T. Biocompatible luminescent silicon quantum dots for imaging of cancer cells. *ACS Nano*. 2008;2(5): 873–878. https://doi.org/10.1021/nn700319z

6. Morozova S., Alikina M., Vinogradov A., Pagliaro M. Silicon quantum dots: synthesis, encapsulation, and application in light-emitting diodes. *Frontiers in Chemistry*. 2020;8: 191. https://doi.org/10.3389/fchem.2020.00191

7. Sobina I. O., Tyurin-Kuzmin P. A., Pervushin N. V., ... Osminkina L. A. Gold-modified silicon microneedles for real-time SERS analysis and drug delivery at single-cell resolution. *Microchemical Journal*. 2025;2015: 114178. https://doi.org/10.1016/j.microc.2025.114178

8. Nazarovskaia D. A., Domnin P. A., Gyuppenen O. D., ... Osminkina L. A. Advanced bacterial detection with SERS-active gold-and silver-coated porous silicon nanowires. *Bulletin of the Russian Academy of Sciences: Physics*. 2023;87(Suppl 1): S41–S46. https://doi.org/10.1134/S1062873823704385

9. Waggoner L. E., Kang J., Zuidema J. M., ... Kwon E. J. Porous silicon nanoparticles targeted to the extracellular matrix for therapeutic protein delivery in traumatic brain injury. *Bioconjugate Chemistry*. 2022;33(9): 1685–1697. https://doi.org/10.1021/acs.bioconjchem.2c00305

10. Osminkina L. A., Timoshenko V. Y. Porous silicon as a sensitizer for biomedical applications. *Open Material Sciences*. 2016;3(1). https://doi.org/10.1515/mesbi-2016-0005

11. Zeng Q., Han K., Zheng C., ... Lu T. Degradable and self-luminescence porous silicon particles as tissue adhesive for wound closure, monitoring and accelerating wound healing. *Journal of Colloid and Interface Science*. 2022;607: 1239–1252. https://doi.org/10.1016/j.jcis.2021.09.092

12. Santos H. A. (ed.). *Porous silicon for biomedical applications (second edition)*. The United Kingdom: Woodhead Publishing; 2021. https://doi.org/10.1016/b978-0-12-821677-4.00007-0

13. Cullis A. G., Canham L. T., Calcott P. D. J. The structural and luminescence properties of porous silicon. *Journal of Applied Physics*. 1997;82(3): 909–965. https://doi.org/10.1063/1.366536

14. Skorb E. V., Andreeva D. V., Möhwald H. Generation of a porous luminescent structure through ultrasonically induced pathways of silicon modification. *Angewandte Chemie International Edition*. 2012;21(51): 5138–5142. https://doi.org/10.1002/anie.201105084

15. Sailor M. J. (ed.). Porous silicon in practice: preparation, characterization and applications. Weinheim, Germany: Wiley-VCH Verlag & Co.; 2011. https://doi.org/10.1002/9783527641901

16. Park J. H., Gu L., von Maltzahn G., Ruoslahti E., Bhatia S. N., Sailor M. J. Biodegradable luminescent porous silicon nanoparticles for in vivo applications. *Nature Materials*. 2009;8: 331–336. https://doi.org/10.1038/nmat2398

17. Gu L., Hall D. J., Qin Z., ... Sailor M. J. In vivo time-gated fluorescence imaging with biodegradable luminescent porous silicon nanoparticles. Nature communications. 2013;4(1): 2326. https://doi.org/10.1038/ncomms3326

18. Shatskaia M. G., Nazarovskaia D. A., Gonchar K. A., ... Osminkina L. A. Photoluminescent porous silicon nanowires as contrast agents for bioimaging. Condensed Matter and Interphases. 2024;26(1): 161–167. https://doi.org/10.17308/kcmf.2024.26/11819

19. Kelly T. L., Gao T., Sailor M. J. Carbon and carbon/silicon composites templated in rugate filters for the adsorption and detection of organic vapors. *Advanced Materials*. 2011;15(23): 1776–1781. https://doi.org/10.1002/adma.201004142

20. Amato G., Brunetto N., Parisini A. Characterisation of freeze-dried porous silicon. *Thin Solid Films*. 1997;297(1-2): 73-78. https://doi.org/10.1016/S0040-6090(96)09412-6

21. Koyuda D. A., Titova S. S., Tsurikova U. A., ... Turishchev S. Yu. Composition and electronic structure of porous silicon nanoparticles after oxidation under air-or freeze-drying conditions. *Materials Letters*. 2022;312: 131608. https://doi.org/10.1016/j.matlet.2021.131608

22. Kim D., Kang J., Wang T., ... Sailor M. J. Two-photon in vivo imaging with porous silicon nanoparticles. *Advanced Materials*. 2017;29(39): 1703309. https://doi.org/10.1002/adma.201703309

23. Stohr J. (ed.). *NEXAFS Spectroscopy*. Berlin, Germany: Springer International Publishing; 1996.

24. Bunker G. (ed.). *Introduction to XAFS*. Cambridge, the United Kingdom: Cambridge University Press; 2010.

25. Barranco A., Yubero F., Espinos J. P., Groening P., Gonzalez-Elipe A. R. Electronic state characterization of SiOx thin films prepared by evaporation. *Journal of Applied Physics*. 2005;97: 113714. https://doi.org/10.1063/1.1927278

26. Liu L., Sham T. K. The effect of thermal oxidation on the luminescence properties of nanostructured silicon. *Small*. 2012;8: 2371–2380. https://doi.org/10.1002/smll.201200175

27. Turishchev S. Yu., Parinova E. V., Pisliaruk A. K., ... Sivakov V. Surface deep profile synchrotron studies of mechanically modified top-down silicon nanowires array using ultrasoft X-ray absorption near edge structure spectroscopy. *Scientific Reports*. 2019;9: 8066. https://doi.org/10.1038/s41598-019-44555-y

28. Parinova E. V., Fedotov A. K., Koyuda D. A., ... Turishchev S. Y. The composite structures based on nickel rods in the matrix of silicon dioxide formation peculiarities study using synchrotron XANES in electrons and photons yield registration modes. *Condensed Matter and Interphases*.2019;21(1): 116–125. https://doi.org/10.17308/kcmf.2019.21/726

29. Lebedev A. M., Menshikov K. A., Nazin V. G., Stankevich V. G., Tsetlin M. B., Chumakov R. G. Nano PES photoelectron beamline of the Kurchatov Synchrotron Radiation Source. *Journal of Surface Investigation: X-ray, Synchrotron and Neutron Techniques*. 2021;15: 1039–1044. https://doi.org/10.1134/S1027451021050335

30. Kasrai M., Lennard W. N., Brunner R. W., Bancroft G. M., Bardwell J. A., Tan K. H. Sampling depth of total electron and fluorescence measurements in Si L- and K-edge absorption spectroscopy. *Applied Surface Science*. 1996;99(4): 303–312. https://doi.org/10.1016/0169-4332(96)00454-0

31. Erbil A., Cargill III G. S., Frahm R., Boehme R. F. Total-electron-yield current measurements for near-surface extended X-ray-absorption fine structure. *Physical Review B*. 1988;37: 2450–2464. https://doi.org/10.1103/PhysRevB.37.2450

32. Mushahary D., Spittler A., Kasper C., Weber V., Charwat V. Isolation, cultivation, and characterization of human mesenchymal stem cells. *Cytometry Part A*. 2018;93(1): 19–31. https://doi.org/10.1002/cyto.a.23242

33. Kulebyakin K., Tyurin-Kuzmin P., Sozaeva L., ... Vorontsova M. Dynamic balance between pth1r-dependent signal cascades determines its pro-or anti-osteogenic effects on MSC. *Cells*. 2022;11(21): 3519. https://doi.org/10.3390/cells11213519

34. Kulebyakin K., Tyurin-Kuzmin P., Efimenko A., ... Tkachuk V. Decreased insulin sensitivity in telomerase-immortalized mesenchymal stem cells affects efficacy and outcome of adipogenic differentiation in vitro. *Frontiers in Cell and Developmental Biology*. 2021;9: 662078. https://doi.org/10.3389/fcell.2021.662078

35. Turishchev S. Yu., Koyuda D. A., Terekhov V. A., ... Domashevskaya E. P. Electronic structure and composition of the surface layers of the multilayer nanoperiodical structures a-Si/ZrO_2 and a-SiOx/ZrO_2 according to synchrotron studies. *Condensed Matter and Interphases*. 2016;18(4): 558–567. (Ib Russ., abstract in Eng.). Available at: https://www.elibrary.ru/item.asp?id=27474862

36. Watanabe M., Ejima T., Miyata N., Imazono T., Yanagihara M. Studies of multilayer structure in depth direction by soft X-ray spectroscopy. *Nuclear Science and Techniques*. 2006;17(5): 257–267. https://doi.org/10.1016/S1001-8042(06)60048-1

37. Turishchev S. Y., Terekhov V. A., Koyuda D. A., ... Mashin A. I. Synchrotron investigation of the multilayer nanoperiodical Al_2O_3/SiO/Al_2O_3/SiO:Si structure formation. *Surface and Interface Analysis*. 2012;44(8): 1182-1186. https://doi.org/10.1002/sia.4868

38. Turishchev S. Y., Parinova E. V., Pisliaruk A. K., ... Sivakov V. Surface deep profile synchrotron studies of mechanically modified top-down silicon nanowires array using ultrasoft X-ray absorption near edge structure spectroscopy. *Scientific Reports*. 2019;9(1): 8066. https://doi.org/10.1038/s41598-019-44555-y

39. Engelhorn K., Recoules V., Cho B. I., ... Heimann P. A. Electronic structure of warm dense silicon dioxide. *Physical Review B*. 2015;91(21): 214305. https://doi.org/10.1103/PhysRevB.91.214305

40. Zi J., Zhang K., Xie X. Comparison of models for Raman spectra of Si nanocrystals. *Physical Review B*. 1997;55(15): 9263. https://doi.org/10.1103/PhysRevB.55.9263

41. Canham L. T. (ed.). *Handbook of porous silicon*. Berlin, Germany: Springer International Publishing; 2018. https://doi.org/10.1007/978-3-319-71381-6

Information about the authors

Darya A. Nazarovskaya, postgraduate Student, Faculty of Physics, Lomonosov Moscow State University (Moscow, Russian Federation).

https://orcid.org/0000-0001-8151-9602

nazarovskaia.da22@physics.msu.ru

Sergey Yu. Turischev, Dr. Sci. (Phys.–Math.), Head of the Department of General Physics and Physical Materials Science, Physics Department, Voronezh State University (Voronezh, Russian Federation).

https://orcid.org/0000-0003-3320-1979

tsu@phys.vsu.ru

Sofia S. Titova, Lecturer, Department of General Physics and Physical Materials Science, Physics Department, Voronezh State University (Voronezh, Russian Federation).

https://orcid.org/0000-0001-6860-401X

titova@phys.vsu.ru

Artur A. Shatov, student, Faculty of Physics, Lomonosov Moscow State University (Moscow, Russian Federation).

mr.ArturSh@mail.ru

Pyotr A. Tyurin-Kuzmin,, Dr. Sci. (Biology), Associate Professor, Faculty of Medicine, Lomonosov Moscow State University (Moscow, Russian Federation); Institute for Biological Instrumentation of the Russian Academy of Sciences (Pushchino, Russian Federation).

https://orcid.org/0000-0002-1901-1637

tyurinkuzminpa@my.msu.ru

Liubov A. Osminkina, Cand. Sci. (Phys.–Math.), Leading Researcher, Faculty of Physics, Lomonosov Moscow State University (Moscow, Russian Federation); Institute for Biological Instrumentation of the Russian Academy of Sciences (Pushchino, Russian Federation).

https://orcid.org/0000-0001-7485-0495

osminkina@physics.msu.ru

Received October 17, 2024; approved after reviewing October 30, 2024; accepted for publication November 15, 2024; published online September 25, 2025.